

# SCIENTIFIC REPORTS

OPEN

## Singlet oxygen imaging using fluorescent probe Singlet Oxygen Sensor Green in photosynthetic organisms

Ankush Prasad<sup>1</sup>, Michaela Sedlářová<sup>2</sup> & Pavel Pospíšil<sup>1</sup>

Formation of singlet oxygen ( $^1\text{O}_2$ ) was reported to accompany light stress in plants, contributing to cell signaling or oxidative damage. So far, Singlet Oxygen Sensor Green (SOSG) has been the only commercialized fluorescent probe for  $^1\text{O}_2$  imaging though it suffers from several limitations (unequal penetration and photosensitization) that need to be carefully considered to avoid misinterpretation of the analysed data. Herein, we present results of a comprehensive study focused on the appropriateness of SOSG for  $^1\text{O}_2$  imaging in three model photosynthetic organisms, unicellular cyanobacteria *Synechocystis* sp. PCC 6803, unicellular green alga *Chlamydomonas reinhardtii* and higher plant *Arabidopsis thaliana*. Penetration of SOSG differs in both unicellular organisms; while it is rather convenient for *Chlamydomonas* it is restricted by the presence of mucoid sheath of *Synechocystis*, which penetrability might be improved by mild heating. In *Arabidopsis*, SOSG penetration is limited due to tissue complexity which can be increased by pressure infiltration using a shut syringe. Photosensitization of SOSG and SOSG endoperoxide formed by its interaction with  $^1\text{O}_2$  might be prevented by illumination of samples by a red light. When measured under controlled conditions given above, SOSG might serve as specific probe for detection of intracellular  $^1\text{O}_2$  formation in photosynthetic organisms.

Singlet oxygen ( $^1\text{O}_2$ ) formation is known as a distinctive functional response of organisms to stress stimuli. In plant cells, it has been linked mainly to high light<sup>1–4</sup> but it has been known to occur also in other types of abiotic stress as high temperature, wounding or heavy metals<sup>5</sup>. At high light,  $^1\text{O}_2$  is formed by triplet-triplet energy transfer from triplet chlorophyll to molecular oxygen formed either by change in the spin orientation and charge recombination of the triplet radical pair<sup>3</sup> [ $\text{P680}^{*\text{+}}\text{Pheo}^{*\text{-}}$ ] in the antennae complex and the reaction centre of photosystem II (PSII)<sup>6–8</sup>. Under high temperature and wounding,  $^1\text{O}_2$  was shown to be formed by triplet-triplet energy transfer from triplet carbonyls to molecular oxygen formed during lipid peroxidation<sup>9–11</sup>. The role of  $^1\text{O}_2$  in plant organism is ambivalent; under moderate stress,  $^1\text{O}_2$  appears to act in retrograde signaling pathways<sup>12–14</sup>, whereas under severe stress, it causes oxidative damage of proteins and lipids<sup>15–17</sup>. At low  $^1\text{O}_2$  concentrations, retrograde signaling is associated with acclimation response, whereas at high  $^1\text{O}_2$  concentrations it is accompanied by programmed cell death<sup>13</sup>.

Several spectroscopic and microscopic techniques have been used to detect  $^1\text{O}_2$  formation in photosynthetic organisms both *in vitro* and *in vivo*<sup>2,18,19</sup>. Whereas *in vitro*  $^1\text{O}_2$  detection affords information on the quantification of  $^1\text{O}_2$  formation, *in vivo* techniques provide evidence on the spatiotemporal characterization of  $^1\text{O}_2$  within the plant cells. *In vitro*  $^1\text{O}_2$  detection comprises  $^1\text{O}_2$  phosphorescence, chemical trapping, and spin probe methods. Direct detection of  $^1\text{O}_2$  by phosphorescence at 1270 nm and chemical trapping based on  $\text{O}_2$  uptake due to the reaction of  $^1\text{O}_2$  with histidine or imidazole are feasible solely in isolated PSII reaction centres<sup>3</sup>. Spin probe technique based on the oxidation of diamagnetic nitroxide to paramagnetic nitroxyl radical detected by electron paramagnetic spectroscopy (EPR) is possible in PSII membranes, thylakoids and chloroplasts<sup>20–22</sup>. *In vivo*  $^1\text{O}_2$  detection includes cytochemical techniques using fluorescent and chemiluminescent probes combined with microscopic imaging<sup>23</sup>. In the last two decades, dansyl-based (DanePy)<sup>24</sup> and Singlet Oxygen Sensor Green

<sup>1</sup>Department of Biophysics, Centre of the Region Haná for Biotechnological and Agricultural Research, Faculty of Science, Palacký University, Šlechtitelů 27, 783 71, Olomouc, Czech Republic. <sup>2</sup>Department of Botany, Faculty of Science, Palacký University, Šlechtitelů 27, 783 71, Olomouc, Czech Republic. Ankush Prasad and Michaela Sedlářová contributed equally. Correspondence and requests for materials should be addressed to P.P. (email: [pavel.pospisil@upol.cz](mailto:pavel.pospisil@upol.cz))

reagent<sup>®</sup> (SOSG)<sup>9</sup> fluorescent probes based on the formation of endoperoxides were used to monitor <sup>1</sup>O<sub>2</sub> formation in photosynthetic organisms. These probes are composed of an anthracene moiety (electron donor) that quenches the fluorescence of the fluorochrome (electron acceptor) through electron transfer. Once the anthracene moiety traps <sup>1</sup>O<sub>2</sub>, the resultant oxygen adduct fails to be functional intramolecular electron donor and the fluorescence is recovered.

Singlet Oxygen Sensor Green has been released and tested on plants since mid-2000's<sup>9,23</sup>. Unlike other available fluorescent and chemiluminescent <sup>1</sup>O<sub>2</sub> probes, SOSG fulfils the requirement of high selectivity and specificity. It does not show an appreciable response to superoxide anion radical (O<sub>2</sub><sup>•-</sup>) or hydroxyl radical (HO<sup>•</sup>) which is important especially in chloroplasts where a wide range of ROS are formed<sup>4</sup>. This fluorescein-based dye probe initially exhibits weak blue fluorescence at 395 and 416 nm, under excitation at 372 and 393 nm, respectively. Upon reaction with <sup>1</sup>O<sub>2</sub>, the imminent product SOSG endoperoxide (SOSG-EP) provides green fluorescence, with the excitation and emission maxima lie, based on several authors, in the range of 504–508 nm and 525–536 nm, respectively<sup>25–27</sup>. Spectral properties of SOSG are similar to those of fluorescein which made this probe suitable for observation with a wide range of fluorescence and confocal microscope systems equipped with standard filters.

However, SOSG is known to have several drawbacks (unequal penetration and photosensitization) that must be taken into consideration. SOSG was introduced as a cell-impermeable probe but later studies shown its localization in most cell compartments under different stress conditions<sup>9,23,28</sup>. Further constraints of SOSG application in light-dependent studies is due to its photosensitization. It was demonstrated that SOSG can generate <sup>1</sup>O<sub>2</sub> under exposure to UV radiation (355 nm) and visible light (532 nm), respectively<sup>25</sup>. Later, it was shown that SOSG-EP can serve as photosensitizer even with much higher efficiency than SOSG<sup>26</sup>. A detailed study on SOSG photochemistry showed that singlet excited SOSG converts to triplet excited SOSG via intersystem crossing which further transfers the triplet excitation energy to molecular oxygen forming <sup>1</sup>O<sub>2</sub><sup>27</sup>.

Due to the SOSG and SOSG-EP photosensitization, an effort was initiated to discover fluorescent probe characterized by specificity and sensitivity similar to SOSG; however, lacking its negative trait of photosensitization<sup>25</sup>. Pedersen and co-workers discovered and applied on mammalian cells, a modified <sup>1</sup>O<sub>2</sub> indicator called Aarhus Sensor Green (ASG) (a tetrafluoro-substituted fluorescein derivative covalently linked to a 9,10-diphenyl anthracene moiety)<sup>29</sup>. Aarhus Sensor Green is characterized by spectral properties similar to SOSG omitting its negative trait of photosensitization. Nevertheless, ASG has neither been tested on plants nor available for routine applications. Thus developing new <sup>1</sup>O<sub>2</sub> sensors remained a goal of research teams. In chemical systems, more alternatives to SOSG exist, including FRET-based ratiometric monitoring of <sup>1</sup>O<sub>2</sub> with acene-doped conjugated polymer nanoparticles<sup>30</sup> or <sup>1</sup>O<sub>2</sub> detection in solutions by Bodipy-based energy transfer cassette<sup>31</sup>. Recently, Tang *et al.*<sup>32</sup> proposed an alternative indocyanine green (ICG), a near-infrared (NIR) tricyanocyanine probe that is decomposed after reaction with <sup>1</sup>O<sub>2</sub>. However, the absorption and emission peaks of ICG at ~807 nm and ~822 nm, respectively, make it less convenient for the fluorescence microscopy.

The present study deals with the re-examination of SOSG properties for its possible utilization in model photosynthetic organisms (cyanobacteria, algae, and higher plants) under high light. Penetration of SOSG into the cells can be enhanced by mild heating (cyanobacteria) or moderate-pressure tissue infiltration (higher plants) under conditions avoiding <sup>1</sup>O<sub>2</sub> formation by high temperature or leaf wounding itself. Illumination by a red light ( $\lambda \geq 600$  nm) is advised to avoid <sup>1</sup>O<sub>2</sub> formation due to SOSG and SOSG-EP photosensitization. As the experimental conditions may significantly affect the obtained results, we attempt to summarize the principal factors that must be taken into account when imaging <sup>1</sup>O<sub>2</sub> with SOSG in photosynthetic organisms.

## Material and Methods

**Plant material.** *Synechocystis* sp. (PCC 6803) was grown in BG-11 medium supplemented with 5 mM glucose and 5 mM sodium bicarbonate as the main carbon source under a continuous white light (100  $\mu$ mol photons m<sup>-2</sup> s<sup>-1</sup>) at 25 °C<sup>33</sup>. The cell culture was permanently stirred using magnetic stirrer RT 5 power (IKA Werke GmbH, Staufen, Germany) to obtain a constant CO<sub>2</sub> concentration in the growth medium. The cells from the end of log phase at a density of approximately 10<sup>8</sup>–10<sup>9</sup> cells ml<sup>-1</sup> were used for experiments. *Chlamydomonas reinhardtii* (CC-002) was obtained from the Chlamydomonas Genetic Center (Duke University, Durham, NC, USA). The cells were cultivated in Tris-Acetate-Phosphate (TAP) medium or in Bold's basal medium (BBM) in a continuous white light (100  $\mu$ mol photons m<sup>-2</sup> s<sup>-1</sup>) in Algaetron AG 230 (Photon Systems Instruments, Drásov, Czech Republic). The growth was achieved under permanently stirred condition using shaker (Orbital Shaker PSU-10i, Biosan, Riga, Latvia) to obtain a constant CO<sub>2</sub> concentration in the growing medium<sup>10,34</sup>. The cells were studied at a density of approximately 7 × 10<sup>7</sup> cells ml<sup>-1</sup> during the stationary growth phase. *Arabidopsis thaliana* (Col-0) seeds from the Nottingham Arabidopsis Stock Centre (NASC) were soaked in distilled water for 4 days at 4 °C and transferred into the growing pots filled with a peat substrate (Klasmann, Potground H). The plants were grown for 4–6 weeks in a growing chamber at a photoperiod of 8/16 h light/dark (100  $\mu$ mol photons m<sup>-2</sup> s<sup>-1</sup>) at a temperature of 22 °C/20 °C, respectively and relative humidity 60%.

**SOSG staining.** *Synechocystis* cells (BG-11 medium, pH 7.1), *Chlamydomonas* cells (TAP medium, pH 7.0 or BBM medium pH 6.8) and *Arabidopsis* leaf pieces with adaxial side of leaf up (5 × 5 mm, HEPES pH 7.5) were placed in 2 ml Eppendorf tube and treated with 50  $\mu$ M SOSG (Molecular Probes Inc., Eugene, OR, USA) for 30 min either in dark or exposed to light. For *Synechocystis* and *Chlamydomonas* cells, the media containing SOSG was replaced with growing medium before measurement while for *Arabidopsis* leaf, the measurement was done in pure buffer.

**High light.** The illumination was performed using a LED source with a light guide CL6000 LED Zeiss (Carl Zeiss Microscopy GmbH, Jena, Germany). Samples were exposed to continuous white light ( $\lambda = 400$ –750 nm) or

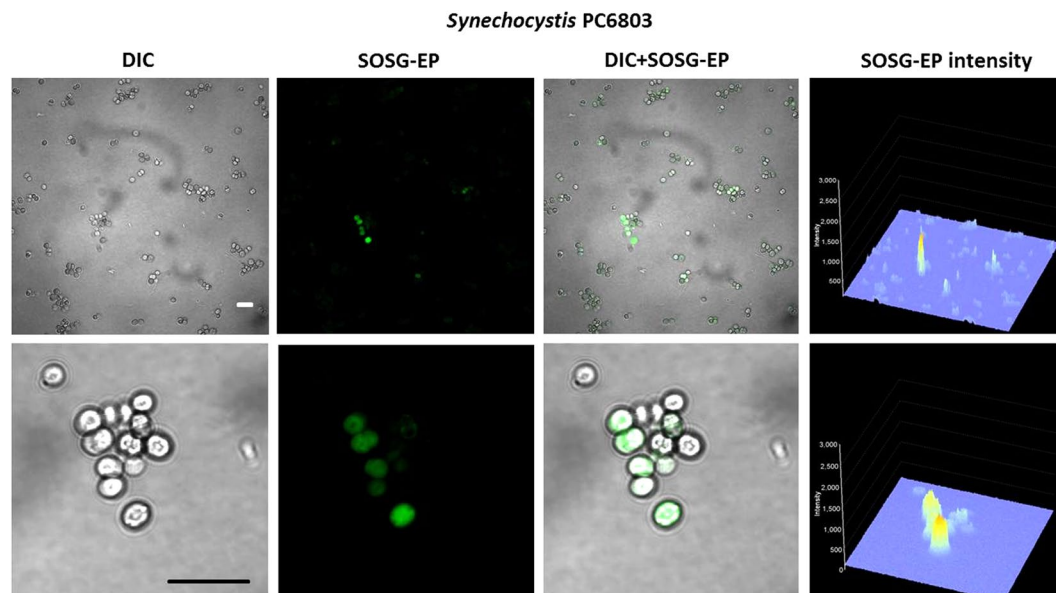


**Figure 1.** Singlet oxygen imaging in *Synechocystis* cells. *Synechocystis* cells were exposed to red light for 30 min in the presence of 50  $\mu\text{M}$  SOSG and at 37  $^{\circ}\text{C}$ . From left to right: Nomarski DIC, SOSG-EP fluorescence ( $\lambda_{\text{em}} = 505\text{--}525\text{ nm}$ ) and combined channel (DIC + SOSG-EP). Bar in both the upper and the lower panel represents 5  $\mu\text{m}$ .

red light ( $\lambda \geq 600\text{ nm}$ ) with an intensity of  $1000\ \mu\text{mol photons m}^{-2}\ \text{s}^{-1}$  transferred by optical fiber guide to the top of Eppendorf tube. Long-pass edge interference filter (600 nm) (Andover Corporation, Salem, NH, USA) was used to cut off the blue-green region of the spectra.

**Fluorescence emission spectra.** Fluorescence emission spectra were measured using a fluorescence spectrometer F-4500 (Hitachi, Tokyo, Japan). For fluorescence emission spectra, the SOSG was excited at 488 nm and SOSG-EP fluorescence was recorded in the spectral range of 500–640 nm.

**Singlet oxygen imaging by confocal laser scanning microscopy.** Immediately after staining, the cells were transferred to corresponding fresh media and visualized by confocal laser scanning microscopy (Fluorview 1000 unit attached to IX80 microscope; Olympus Czech Group, Prague, Czech Republic). The excitation of SOSG was performed by a 488 nm line of an argon laser and the emission was detected by a 505–525 nm filter. Cell morphology was visualized by transmitted light detection module with 405 nm excitation using a near ultraviolet (405 nm) diode laser and differential interference contrast (DIC) filters. The proper intensity of all lasers was set according to unstained samples at the beginning of each experiment<sup>35</sup>. Integral distribution of signal intensity (0–4096) in 12-bit microphotographs was evaluated by image analysis software FV10-ASW 4.0 Viewer (Olympus).

## Results

**SOSG penetration.** To monitor  $^1\text{O}_2$  formation in unicellular photosynthetic organisms, SOSG-EP fluorescence was detected in *Synechocystis* (Figs 1–3) and *Chlamydomonas* (Fig. 4) cells by confocal laser scanning microscopy. Figures 1 and 4 demonstrate Nomarski DIC channel (greyscale), fluorescence channel (green), the combination of both channels and the integral distribution of the signal intensity within the sample. When *Synechocystis* cells were exposed to red light in the presence of SOSG, SOSG-EP fluorescence was observed. Detail focus shows that SOSG-EP fluorescence is distributed uniformly in the whole cell (Fig. 1). Similarly, exposure of *Chlamydomonas* cells to red light resulted in the appearance of SOSG-EP fluorescence localized predominantly within the chloroplasts (Fig. 4). Whereas the penetration of SOSG into the *Chlamydomonas* cells has no serious limitation and uptake can be achieved by the placement of cells in the dye, the penetration of SOSG into the *Synechocystis* cells is restricted due to the presence of polysaccharide matrix forming mucous surface structures. Figure 2 shows that SOSG penetration into the *Synechocystis* cells is improved largely by mild heating (37  $^{\circ}\text{C}$ ) known to dissolve mucoid sheath. As mild heating of *Synechocystis* cells did not enhance SOSG-EP fluorescence in dark (data not shown), it indicates that mild heating to 37  $^{\circ}\text{C}$  causes no  $^1\text{O}_2$  formation by lipid peroxidation initiated by lipoxygenase as previously shown in *Chlamydomonas* exposed to 40  $^{\circ}\text{C}$ <sup>10</sup>. Figure 3 (red circle) shows that some cells exhibit SOSG-EP fluorescence from the outer regions of the cell. A series of optical sections through the cells reveals that SOSG is uniformly spread out in these cells and SOSG-EP fluorescence from the outer regions of the cell is due to the plane of focus. In order to confirm that observed SOSG-EP fluorescence enhancement is due to  $^1\text{O}_2$  generation, the effect of scavengers of  $^1\text{O}_2$  (sodium azide/histidine) was measured in *Chlamydomonas* cells exposed to red light. A considerable suppression in SOSG-EP fluorescence was observed (see Supplementary Figs S4–S5).

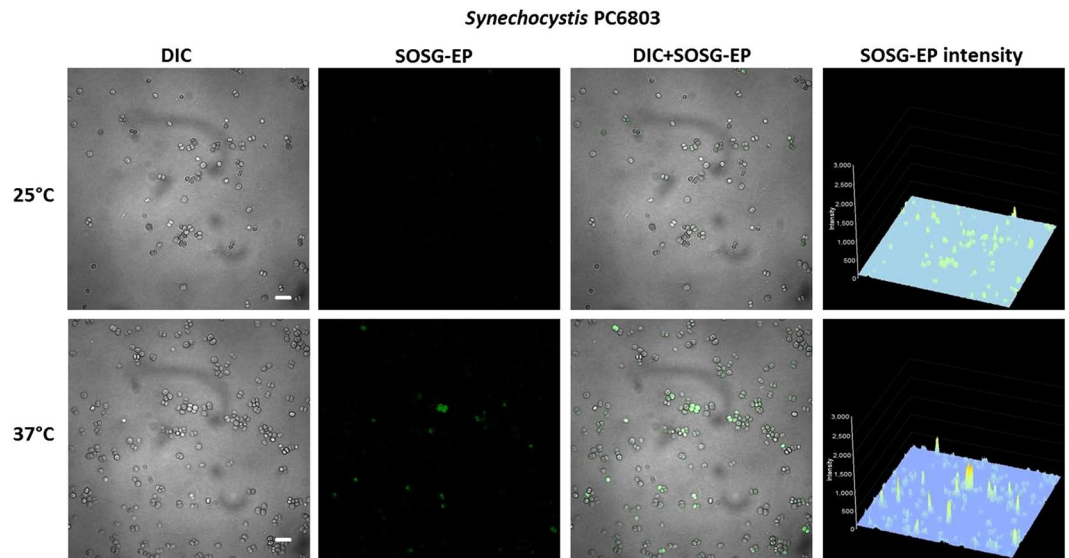


**Figure 2.** Effect of mild heating on the penetration of SOSG into the *Synechocystis* cells. *Synechocystis* cells were exposed to red light for 30 min in the presence of 50  $\mu$ M SOSG at the temperature (25 °C) (upper panel) and (37 °C) (lower panel). From left to right are Nomarski DIC, SOSG-EP fluorescence ( $\lambda_{em} = 505\text{--}525$  nm) and combined channel (DIC + SOSG-EP). Bar represents 5  $\mu$ m.

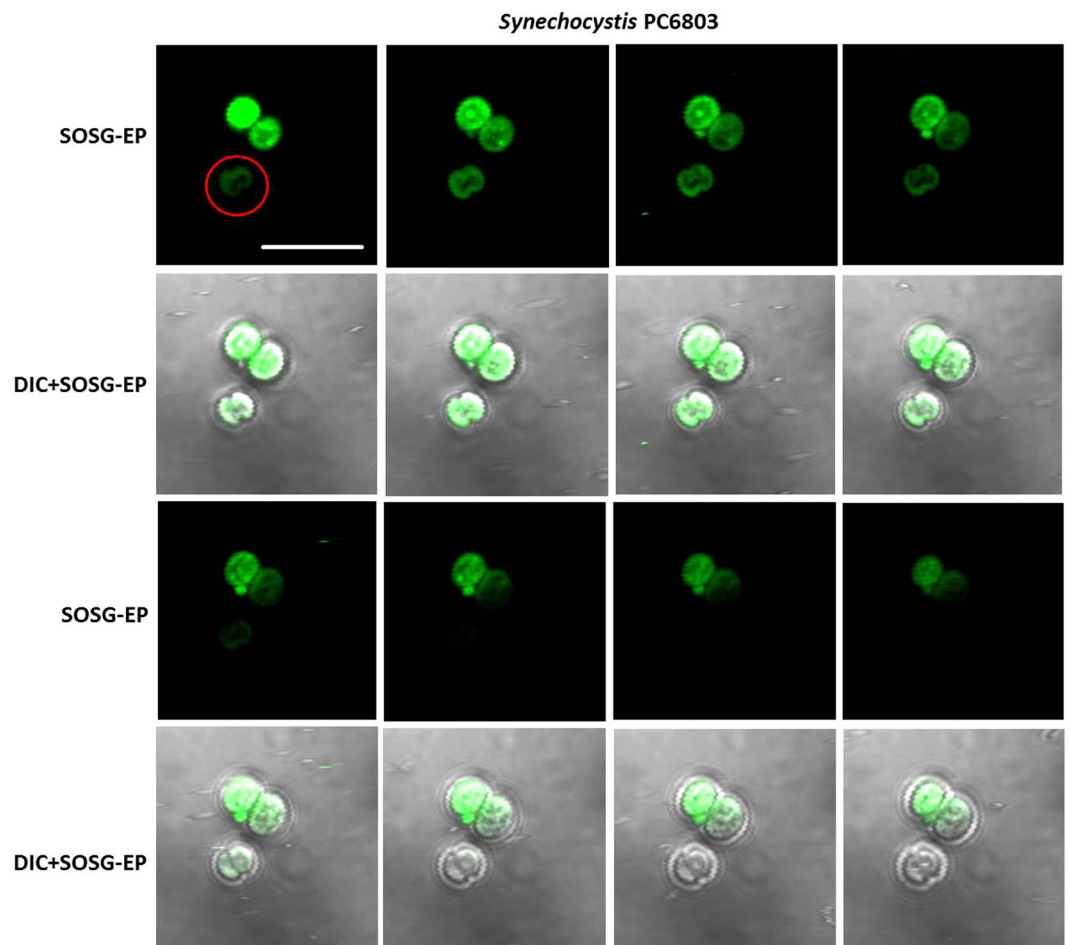


**Figure 3.** Series of optical sections through *Synechocystis* cells. Red circle shows SOSG-EP fluorescence at the outer regions of the cell. SOSG-EP and DIC + SOSG-EP channel channels are shown. Bar represents 5  $\mu$ m. Other experimental conditions as in Fig. 1.

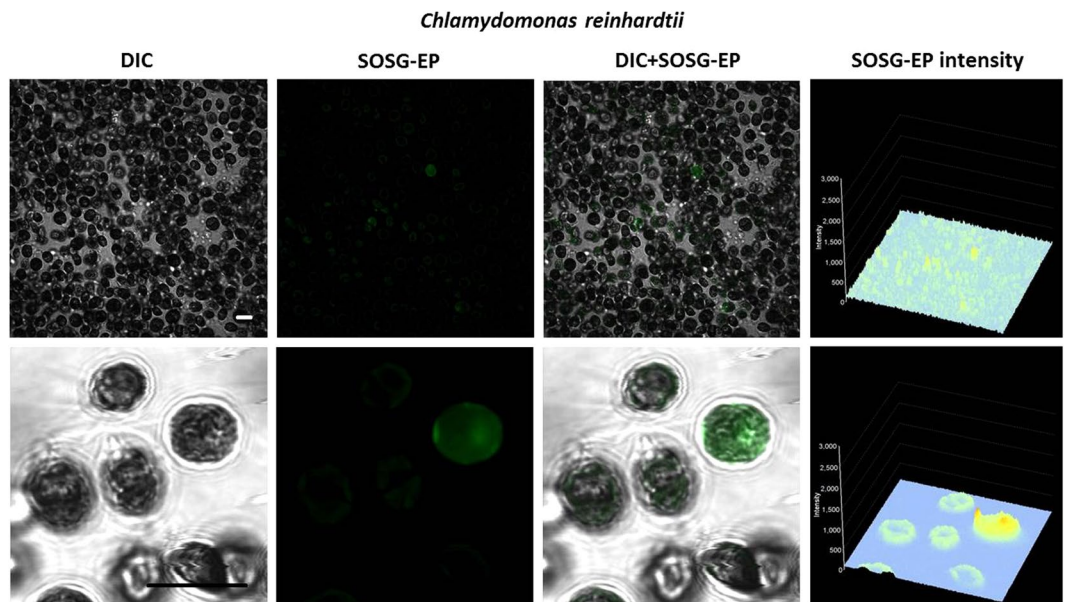


**Figure 4.** Singlet oxygen imaging in *Chlamydomonas* cells. *Chlamydomonas* cells were exposed to red light for 30 min in the presence of 50  $\mu\text{M}$  SOSG. From left to right: Nomarski DIC, SOSG-EP fluorescence ( $\lambda_{\text{em}} = 505\text{--}525\text{ nm}$ ) and combined channel (DIC + SOSG-EP). Bar represents 10  $\mu\text{m}$ .

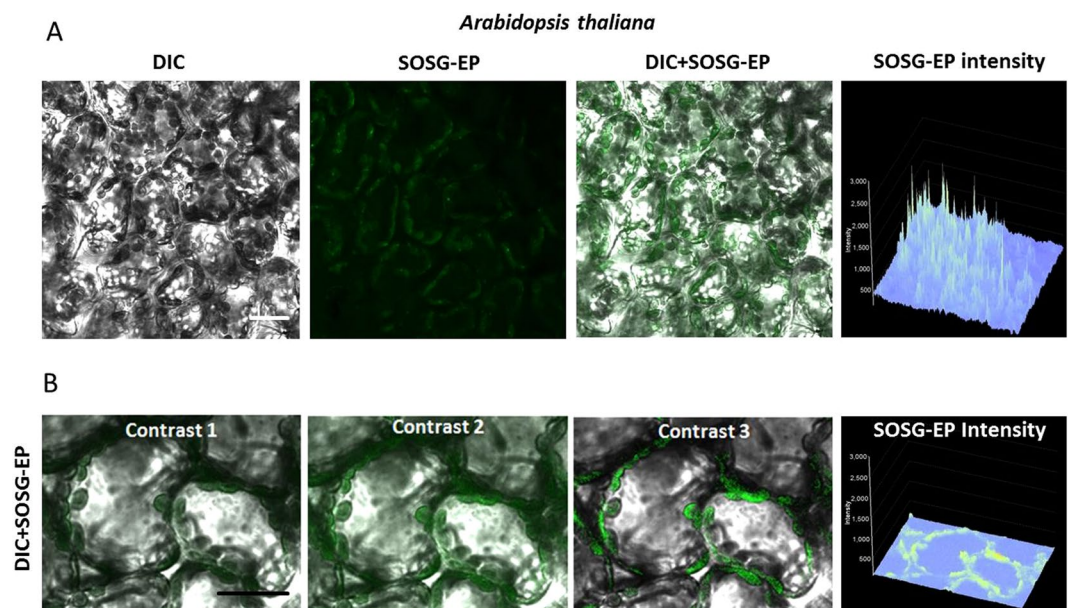


**Figure 5.** Singlet oxygen imaging in *Arabidopsis* leaves. (A) *Arabidopsis* leaves were exposed to red light for 30 min in the presence of 50  $\mu\text{M}$  SOSG. From left to right: Nomarski DIC, SOSG-EP fluorescence ( $\lambda_{\text{em}} = 505\text{--}525\text{ nm}$ ) and combined channel (DIC + SOSG-EP). (B) Example of post-processing signal-to-noise ratio applied to a 12-bit figure (*Arabidopsis*, 50  $\mu\text{M}$  SOSG, 30 min, red light, DIC + SOSG-EP fluorescence channel at 505–525 nm). SOSG-EP fluorescence was emphasized by limiting shades to 0–1500 or 50–1000 and increasing contrast of SOSG-EP channel from 1, 2 and 3. Bar represents 20  $\mu\text{m}$ .

Light-induced formation of  $^1\text{O}_2$  was accordingly visualized with SOSG in *Arabidopsis* leaves (Fig. 5). When *Arabidopsis* leaves were exposed to red light in the presence of SOSG, the SOSG-EP fluorescence was detected predominantly from the chloroplasts located at the periphery of the mesophyll cells (Fig. 5A). Figure 5B shows a series of SOSG-EP fluorescence at limiting shades [0–1500 or 50–1000] and increasing contrast of SOSG-EP channel [contrast range: 1–3]. In *Arabidopsis* leaves, SOSG penetration is limited due to the tissue complexity comprising the upper and lower epidermis covered by cuticle. Penetration of SOSG into the mesophyll cells can be achieved through cutting edge (to a less extent by stomata) by pressure infiltration using the shut syringe. The

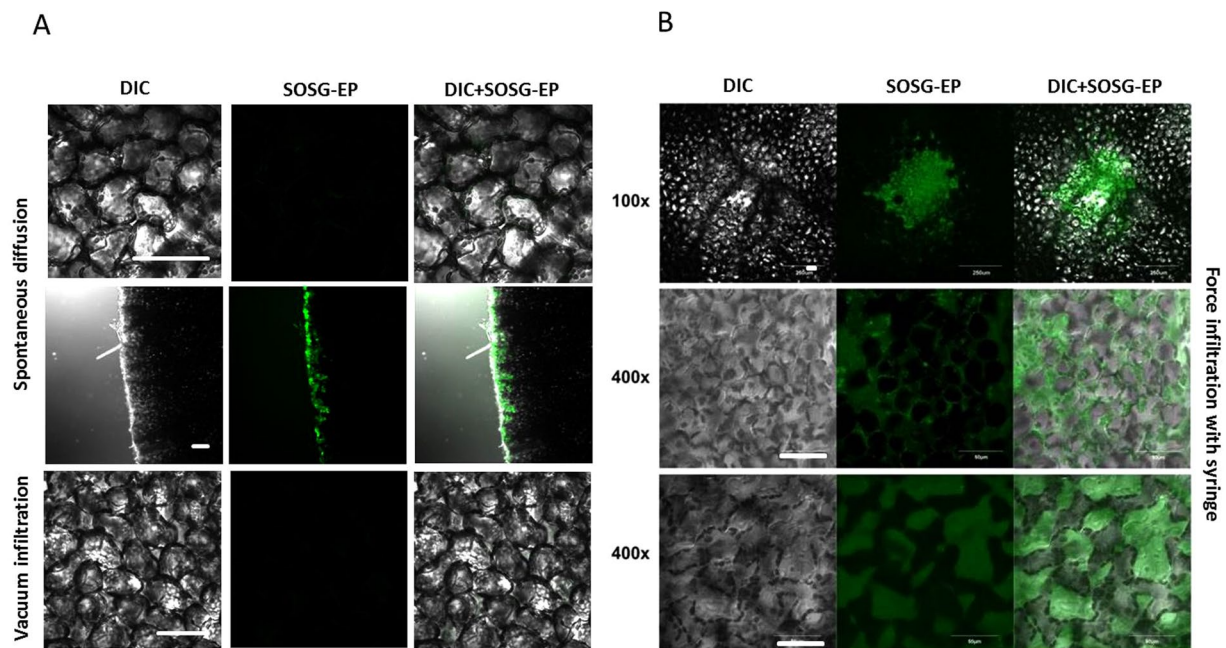


**Figure 6.** SOSG infiltration into Arabidopsis leaves. (A) Spontaneous diffusion measured at the centre of the excised leaf (upper row), spontaneous diffusion measured at the cut edges (middle row) and vacuum infiltration (lower row). (B) Force infiltration with a syringe. The image with resolution 100x shows the mechanical injury at the site of force infiltration and 400x magnification are focused on layers of sponge and below on palisade parenchyma cells. In A and B, from left to right are Nomarski DIC, fluorescence ( $\lambda_{em} = 505\text{--}525\text{ nm}$ ) and combined (DIC + SOSG) channel. Bar represents 50  $\mu\text{m}$ .

efficiency of SOSG penetration into the mesophyll cells depends on several factors including the leaf age and water content within the tissue (data not shown). This approach is efficient in the uniform delivery of SOSG into the mesophyll cells and gentle with respect to mechanical injury known to cause  $^1\text{O}_2$  formation as previously shown in Arabidopsis leaves<sup>11</sup>. Different approaches such as spontaneous diffusion measured either at the centre of the excised leaf or at cut edges and vacuum infiltration were used; however, no penetration or uneven penetration was possible to be achieved (Fig. 6A). Furthermore, force infiltration with syringe results in the uneven delivery of SOSG to the mesophyll cells and the leaf injury at the site of puncture. Figure 6B shows that penetration into the tissues is inconsistent, randomly distributed in the both intercellular and extracellular spaces. The mechanical injury provides the highest signal in the centre (100x magnification) and influences results of staining upon stress treatment (at 400x magnification focused on layers of sponge and below on palisade parenchyma cells).

To confirm that SOSG penetrates uniformly into the cells, 3-D distribution of SOSG-EP fluorescence within cells or tissues was visualized by Z-stacks of thin optical sections. Figure 7 shows a series of 5 optical sections with a distance of 0.5  $\mu\text{m}$  (Synechocystis cells), 1  $\mu\text{m}$  (Chlamydomonas cells) and 4  $\mu\text{m}$  (Arabidopsis leaves), respectively. SOSG-EP fluorescence measured in the multiple layers in Synechocystis and Chlamydomonas cells were observed from overall cell volume with fluorescence intensity higher at the cell periphery. In Arabidopsis leaves, SOSG-EP fluorescence comes predominantly from the chloroplasts located at the periphery of the cells. These results show that penetration of the probe (at the depth of cells and tissues) can be reached with a proper modified procedure of staining.

**SOSG photosensitization.** To test the photosensitization of SOSG and SOSG-EP, the probe was first illuminated in the absence of sample either with red ( $\lambda \geq 600\text{ nm}$ ) or white (400–750 nm) light (Fig. 8). Figure 8A shows SOSG/SOSG-EP fluorescence detected by confocal laser scanning microscopy. When SOSG was kept in dark or exposed to red light, negligible SOSG-EP fluorescence was detected. On the contrary, exposure of SOSG to white light resulted in pronounced SOSG-EP fluorescence. Figure 8B shows SOSG/SOSG-EP fluorescence spectra with an emission maximum at 535 nm measured using fluorescence spectrometer. When SOSG was exposed to white light, SOSG-EP fluorescence was several folds higher compared to red light. Based on these results, it is concluded that red light did not cause  $^1\text{O}_2$  formation due to the photosensitization of SOSG and SOSG-EP, whereas white light resulted in SOSG and SOSG-EP photosensitization. In further, SOSG was illuminated either with red or white light in Synechocystis cells (Fig. 9), Chlamydomonas cells (Fig. 10) and Arabidopsis leaves (Fig. 11) (also see Supplementary Figs S1–S3). In the dark, negligible SOSG-EP fluorescence was due to excitation of SOSG probe by a laser beam,  $^1\text{O}_2$  formation by excitation of photosynthetic pigments by a laser beam and/or dark  $^1\text{O}_2$  formation due to the spontaneous oxidative processes. When Synechocystis (Fig. 9) and Chlamydomonas (Fig. 10) cells were exposed to white light, SOSG-EP fluorescence was enhanced as compared to red light. Similarly, when Arabidopsis leaves were exposed to white light, the intensity of SOSG-EP fluorescence

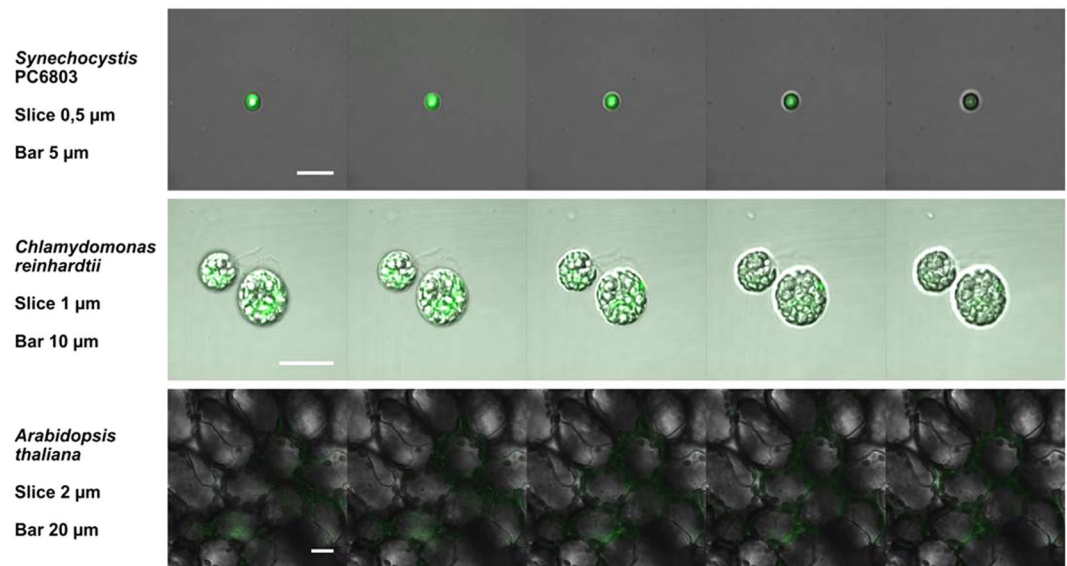


**Figure 7.** Series of optical sections through cells of *Synechocystis*, *Chlamydomonas*, and tissues of *Arabidopsis* leaves. Other experimental conditions as in Figs 1, 4 and 5.

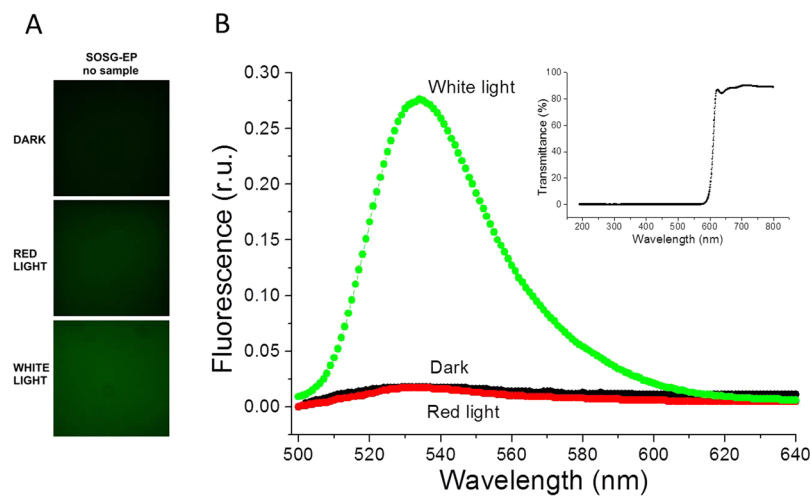


**Figure 8.** Effect of red and white light on SOSG photosensitization. **(A)** SOSG/SOSG-EP fluorescence after exposure of SOSG to red/white light monitored by confocal laser scanning microscopy. **(B)** SOSG/SOSG-EP fluorescence emission spectra after exposure of SOSG to red or white light measured using fluorescence spectrometer. In A and B, SOSG (50  $\mu\text{M}$  in A and 1  $\mu\text{M}$  in B) was kept in dark or illuminated either with red ( $\geq 600$  nm) or white light (400–750 nm) ( $1000 \mu\text{mol photons m}^{-2} \text{s}^{-1}$ ) for 30 min in the absence of any biological sample. SOSG/SOSG-EP fluorescence was produced by excitation at 488 nm and emission was measured in spectral range 505–525 nm **(B)** and 500–640 nm **(B)**. SOSG was dissolved in 40 mM HEPES buffer (pH 7.5) containing 1% methanol. Insert shows transmission spectrum of long-pass edge filter measured using Specord 250 Plus (Analytik Jena AG, Germany).

was higher compared to red light (Fig. 11). These results show that exposure of SOSG to white light causes SOSG and SOSG-EP photosensitization.

## Discussion

In the current study, the use of SOSG for monitoring of  $^1\text{O}_2$  formation was tested in three model photosynthetic organisms. It can be mentioned that despite being tested for numerous applications in the last decade, the exact composition of this probe was not known during initial 5 years of its utilization. Later, Ragas with co-workers showed a combination of fluorescein and anthracene moieties in SOSG by liquid chromatography and UV-VIS spectra, complemented with mass spectrometry and NMR spectroscopy<sup>25</sup>. As the use of SOSG for detection of  $^1\text{O}_2$  formation has a restriction regarding the probe penetration into the cells and probe photosensitization, it is crucial to control the uniform distribution of SOSG in the cells and prevent SOSG photosensitization<sup>36</sup>.

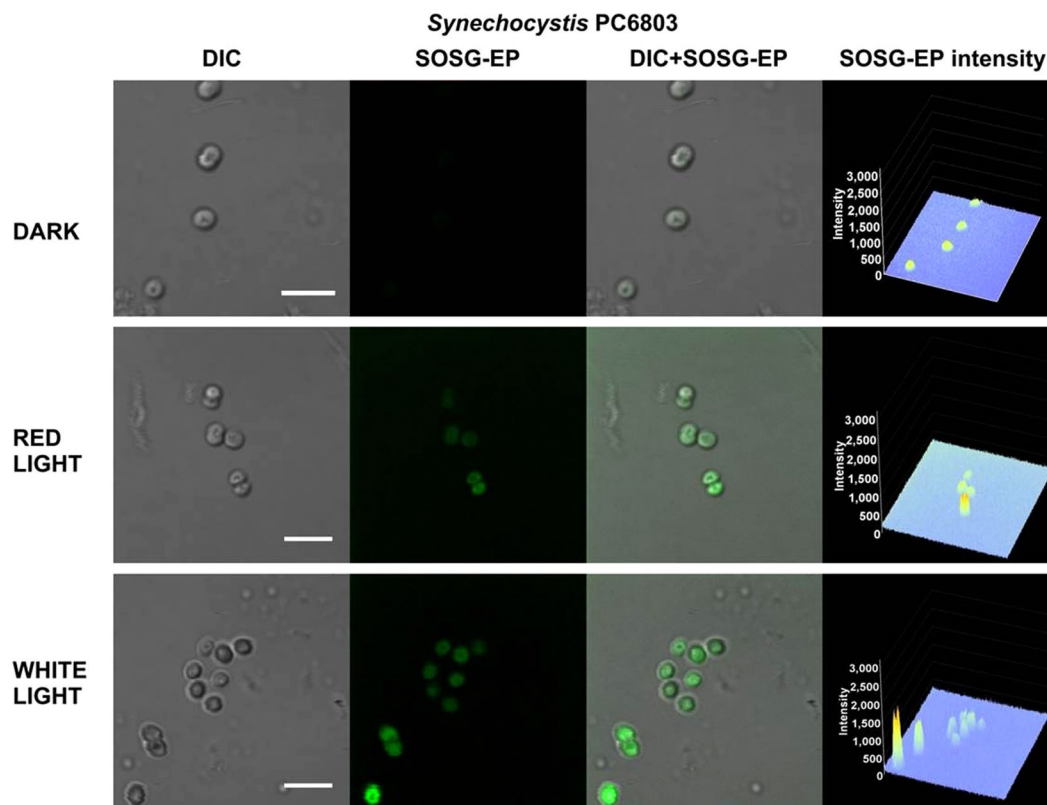


**Figure 9.** Effect of red and white light on singlet oxygen imaging in *Synechocystis* cells. *Synechocystis* cells were treated in 50  $\mu\text{M}$  SOSG for 30 min at 37  $^{\circ}\text{C}$  either in dark or exposed to red/white light. For each treatment following images are presented (from left to right): Nomarski DIC, SOSG-EP fluorescence ( $\lambda_{\text{em}} = 505\text{--}525\text{ nm}$ ), combined channel and integral distribution of the signal intensity within the sample (Z-axis represents the levels of brightness for each pixel, ranging between 0 and 3200). Bar represents 5  $\mu\text{m}$ .

**SOSG permeability.** Penetration of fluorochromes into the plant cells has been a matter of discussions<sup>23,37,38</sup>. SOSG has been claimed as a cell-impermeant substance by the producer<sup>39</sup>; however, experiences acquired during the last decade of its application on biological samples by several research groups proved that it is uptaken by animal cells<sup>26,40</sup>. Unlike animal cells, the presence of cell wall in combination with additional mechanical barriers containing polysaccharide sheath enclosing in the cyanobacteria or cuticle waxes in the plant might hinder delivery of the fluorochrome to the precise organelles of plant cells<sup>38</sup>. Since no diacetate form of SOSG has been available to ease the probe uptake through the plasma membrane, a relatively high concentration (50–250  $\mu\text{M}$ ) and longer incubation periods (30 min) has to be used. Since Flors and co-workers<sup>9</sup> reported the applications of SOSG on diatom species and *Arabidopsis* leaves, several teams employed SOSG in their experiments with unicellular organisms<sup>41</sup> and higher plant<sup>42–46</sup>. SOSG-EP fluorescence visualized in the multiple optical sections through cells of *Synechocystis*, *Chlamydomonas* and *Arabidopsis* confirmed that SOSG penetrates into cells in all tested model photosynthetic organisms (Figs 3 and 7). However, it should be pointed here that confocal laser scanning microscopy has to be used to prove the proper even penetration of the probe into the cells. Detection of  $^1\text{O}_2$  formation exclusively by fluorescence spectrometer might lead to the detection of SOSG-EP fluorescence originating from the extracellular space and thus can be lead to a false signal and misinterpretation of the analysed data.

**SOSG permeability in unicellular organisms.** It is of note that some authors reported that SOSG does not penetrate inside the intact *Synechocystis* cells<sup>47,48</sup>. *Synechocystis* cells are known to excrete polysaccharides to form an outermost slimy layer during cell growth<sup>49</sup>. Penetration of SOSG into the cells enclosed by capsule and mucus might represent a mechanical barrier for SOSG penetration into the *Synechocystis* cells. In this study, we clearly demonstrated that using active cells from the log phase of the growing curve combined with an increase in temperature (37  $^{\circ}\text{C}$  for ca 15 min) as used previously<sup>47</sup> can substantially increase the uptake of SOSG (Figs 1 and 2). It is proposed here that secreting the mucus out of *Synechocystis* cells can decrease SOSG infiltration at later stages of cultivation in liquid media or on agar.

**SOSG permeability in higher plants.** Conversely, higher plants with multiple types of cells and tissues represent a significantly greater challenge. Based on our experiences, the effort to detect intracellular generation of  $^1\text{O}_2$  in multicellular plants can be complicated by uneven staining or mechanical injury during handling with samples. It should be also noted that  $\text{O}_2$ ,  $\text{CO}_2$  and other gases produced by the metabolism of living tissue create



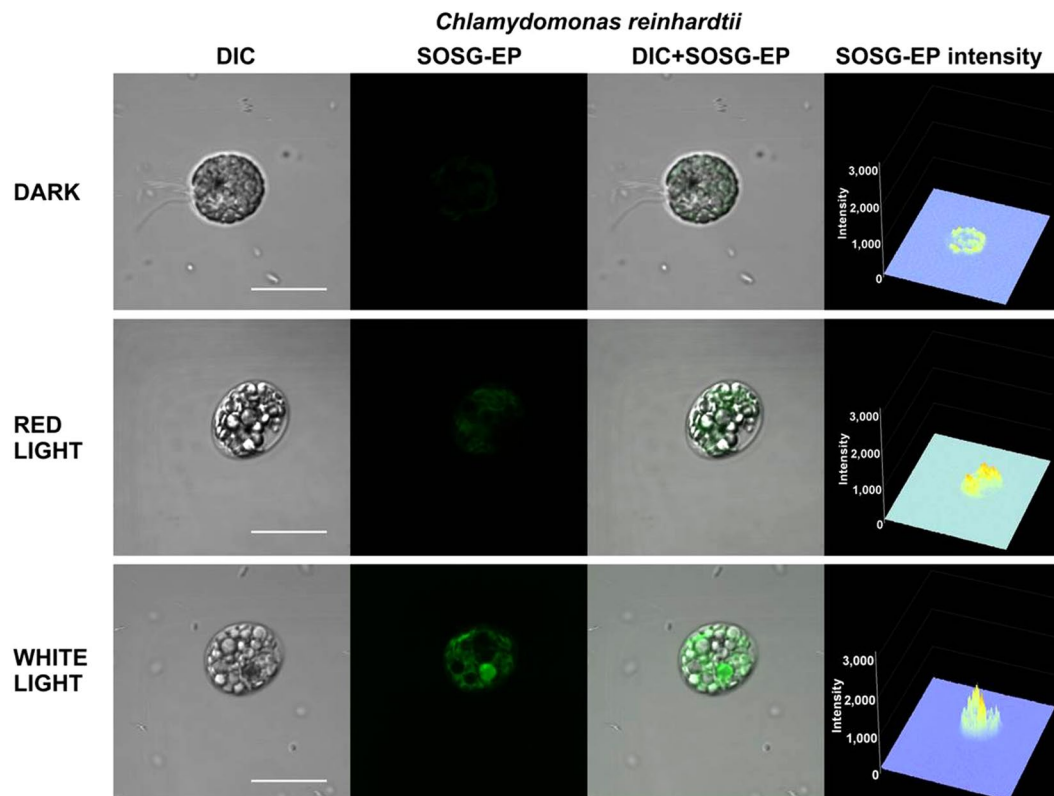


**Figure 10.** Effect of red and white light on singlet oxygen imaging in *Chlamydomonas* cells. *Chlamydomonas* cells were treated in 50  $\mu\text{M}$  SOSG for 30 min either in dark or exposed to red/white light. For each treatment following images are presented (from left to right): Nomarski DIC, SOSG-EP fluorescence ( $\lambda_{\text{em}} = 505\text{--}525\text{ nm}$ ), combined channel and integral distribution of the signal intensity within the sample (Z-axis represents the levels of brightness for each pixel, ranging between 0 and 3200). Bar represents 10  $\mu\text{m}$ .

microbubbles within intercellular space which counteract with uniform sensor delivery to all cells. We have tested several approaches for SOSG infiltration to tissues of *Arabidopsis* leaves comprising spontaneous diffusion, vacuum infiltration, force infiltration with a syringe and pressure infiltration using the shut syringe. Spontaneous diffusion in centre of the excised leaf based on transpiration stream (Fig. 6A, upper row) and vacuum filtration (Fig. 6A, lower row) were found to be with no or uneven distribution of the fluorescent probe. Spontaneous diffusion at cut edges allows uniform distribution of SOSG within several layers of cells from the cut edge (Fig. 6A, middle row). However, the light-induced formation of  $^1\text{O}_2$  was largely overlapped by  $^1\text{O}_2$  formed due to the mechanical injury at the cut edge. It has been recently demonstrated that  $^1\text{O}_2$  is formed by lipid peroxidation initiated by lipoxygenase at the cut edge in the *Arabidopsis* wounding response<sup>11</sup>. The use of spontaneous diffusion at cut edge is possible when 1–3 layers of cells on the cut edge with  $^1\text{O}_2$  formation due to the mechanical injury is excluded from the evaluation. Force infiltration of SOSG with syringe into the leaf tissues through a hole exerted by a needle leads to uneven distribution of the fluorescent probe limited to a leaf mesophyll enclosed by vascular bundles. Furthermore,  $^1\text{O}_2$  is largely formed at the site of hole due to the mechanical injury. The observation that force infiltration of SOSG with syringe is inappropriate is in agreement with previous finding that pinhole infiltration maintains SOSG penetration into the epidermal cells which is unsuitable for study of high light stress<sup>23</sup>. Pressure infiltration using the shut syringe of leaf pieces was found to be both efficient in the uniform distribution of SOSG in the whole sample and unaffected by  $^1\text{O}_2$  formation due to the mechanical injury.

**SOSG photosensitization.** Both SOSG and SOSG-EP were shown to serve as photosensitizers at visible light range<sup>25–27</sup>. In this reaction, singlet excited SOSG formed by excitation of SOSG by visible light passes to the triplet excited SOSG by a change in the orientation of the spin of excited electron via intersystem crossing. Triplet-triplet energy transfer from a triplet excited SOSG to molecular oxygen results in the formation of  $^1\text{O}_2$  and ground state SOSG. Due to these considerations, the relevance of pioneering works published need to be reconsidered cautiously as it might be possible that part of the  $^1\text{O}_2$  was produced by SOSG and SOSG-EP itself.

**SOSG photosensitization in high-light treatment.** Our results demonstrated that SOSG kept in dark or exposed to red light emits only negligible SOSG-EP fluorescence compared to white light (Fig. 8). Similarly, when *Synechocystis* cells (Fig. 9), *Chlamydomonas* cells (Fig. 10) and *Arabidopsis* leaves (Fig. 11) were exposed to white light, pronounced enhancement in SOSG-EP fluorescence was observed as compared to red light. These results demonstrate that a significant increase in SOSG-EP fluorescence upon illumination of SOSG with white

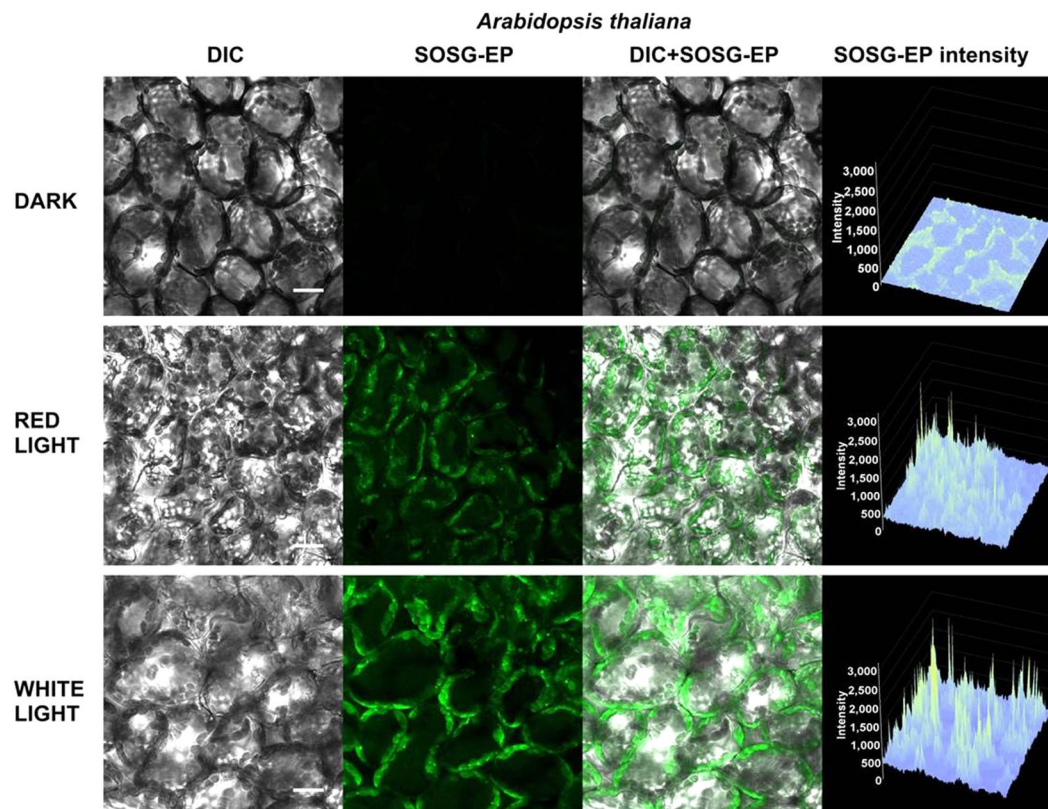


**Figure 11.** Effect of red and white light on singlet oxygen imaging in *Arabidopsis* leaves. *Arabidopsis* leaves were treated in 50  $\mu\text{M}$  SOSG for 30 min either in dark or exposed to red/white light. For each treatment following images are presented (from left to right): Nomarski DIC, SOSG-EP fluorescence ( $\lambda_{\text{em}} = 505\text{--}525\text{ nm}$ ), combined channel and integral distribution of the signal intensity within the sample (Z-axis represents the levels of brightness for each pixel, ranging between 0 and 3200). Bar represents 20  $\mu\text{m}$ .

light is caused by SOSG and SOSG-EP photosensitization. It is proposed that red light led to the formation of  $^1\text{O}_2$  by triplet-triplet energy transfer from excited chlorophyll to molecular oxygen, while white light caused the overall  $^1\text{O}_2$  formation due to the triplet-triplet energy transfer from excited chlorophyll and excited SOSG/SOSG-EP to molecular oxygen.

**SOSG photosensitization during data collection.** Imaging of SOSG and SOSG-EP fluorescence signal is mostly provided by confocal systems employing a 488 nm laser for excitation. However, the complex part of the microscopic study is finding the site of interest within a biological sample. Several authors<sup>23,25</sup> registered an increase of SOSG fluorescence upon exposure to visible radiation. Epifluorescence microscopy of SOSG also utilizes visible light filters but the artefactual SOSG-EP fluorescence can be diminished by a standardized imaging design in which observations under a proper filter, in our case U-MNB-2 (excitation 470–490 nm, emission 520-IF, dichroic at 500 nm), are limited to a minimum time necessary for the only fast sample navigation and focusing.

**SOSG imaging and post-processing techniques.** Synechocystis is characterized by a prokaryotic cell type (i.e. without internal compartmentalization) which size changes over the cell cycle; cells from the logarithmic and stationary phase of growth curve usually reach 1.5–2.5  $\mu\text{m}$  in diameter<sup>50</sup>. Confocal laser scanning microscopy enables detection of the signal from a single focal plane and therefore imaging of more cyanobacterial cells in a single figure might be confusing as it usually includes also cells out of focus. In Chlamydomonas, the presence of flagella exerting algal movement hampers the relatively long confocal imaging. Unfortunately, the requirement of intactness of the cell for *in vivo* studies excludes the use of heat or chemicals used for flagella release. Thus, for unicellular organisms (cyanobacteria, algae) small volumes (ca 5–10  $\mu\text{l}$  under cover slide) of the treated cell suspension can be advised for their immobilization throughout the microscopic observation. To study the 3-D distribution of SOSG-EP fluorescence within cells or tissues, Z-stacks of thin optical sections are employed in confocal microscopy. However, the time vs. resolution during scanning vs. number of optical sections must be compromised to avoid photobleaching. The mode how studied biological matrices affect the outcome of SOSG staining was compared in the three photosynthetic models and SOSG proved to be rather stable, i.e. suitable for multi-layer scans. To verify signal location, particularly in small objects like prokaryotic cells, it is advisable to decrease the pinhole size to 0.9–0.5 airy units, according to signal intensity. Based on the results when SOSG-EP fluorescence was detected in almost all optical sections of the various photosynthetic samples, ranging from

unicellular prokaryote *Synechocystis* to complex tissue structure in *Arabidopsis* leaves, it can be pointed out that SOSG does not suffer from a significant photobleaching compared to other fluorescein probes.

Once collected the whole set of microphotographs (taken under the same standardized conditions) can be post-processed in suitable software to optimize signal-to-noise ratio and thus unable more clear presentation of the signal on screen or in print, particularly for figures with merged channels. This can help especially in 12-bit and 16-bit images, characterized by 4,096 and 65,536 shades, respectively. A universal approach cannot be advised due to the variability of plant materials but the crucial point is to apply the identical algorithm to all variants compared in the experiment to avoid false positive signals. Especially in multi-celled tissues, like *Arabidopsis* leaf sections, the signal location in chloroplasts is better visible after filtering the background and highlighting the SOSG signal in merged figures (Fig. 5B).

## Conclusions

The data presented in this study are expected to contribute to better understanding of the limitation in the use of SOSG for  $^1\text{O}_2$  detection in the photosynthetic organism. Although SOSG penetration into the cell and photosensitization of SOSG by visible light entails the main limitation of SOSG applicability in studies focused on high light stress in the photosynthetic organism, awareness of all the previously mentioned criteria (suitable infiltration procedure and red light) may lead to credible results. When measured under these conditions, SOSG can attend as highly sensitive and specific probe to identify the site of  $^1\text{O}_2$  formation in unicellular photosynthetic organisms and higher plants. However, quantitative analysis of  $^1\text{O}_2$  formation performed exclusively based on SOSG-EP fluorescence images is misleading. Only combination of several methods, e.g. SOSG-EP fluorescence imaging *in vivo* and spin probe EPR spectroscopy *in vitro*, provides comprehensive spatiotemporal and quantitative characterization of  $^1\text{O}_2$  formation in photosynthetic organisms. The different level of  $^1\text{O}_2$  production in different organism can also be attributed to variable cell density, different chlorophyll content, antioxidant level, within the cell/tissues etc. and thus based on the parameters to be evaluated, proper control experiments are required.

## References

- Triantaphylides, C. & Havaux, M. Singlet oxygen in plants: production, detoxification and signaling. *Trends Plant Sci* **14**, 219–228, <https://doi.org/10.1016/j.tplants.2009.01.008> (2009).
- Fischer, B. B., Hideg, E. & Krieger-Liszka, A. Production, Detection, and Signaling of Singlet Oxygen in Photosynthetic Organisms. *Antioxidants & Redox Signaling* **18**, 2145–2162, <https://doi.org/10.1089/ars.2012.5124> (2013).
- Telfer, A. Singlet Oxygen Production by PSII Under Light Stress: Mechanism, Detection and the Protective role of beta-Carotene. *Plant and Cell Physiology* **55**, 1216–1223, <https://doi.org/10.1093/pcp/pcu040> (2014).
- Pospíšil, P. Production of Reactive Oxygen Species by Photo system II as a Response to Light and Temperature Stress. *Frontiers in Plant Science* **7**, 12, <https://doi.org/10.3389/fpls.2016.01950> (2016).
- Pospíšil, P. & Prasad, A. Formation of singlet oxygen and protection against its oxidative damage in Photosystem II under abiotic stress. *Journal of Photochemistry and Photobiology B-Biology* **137**, 39–48, <https://doi.org/10.1016/j.jphotobiol.2014.04.025> (2014).
- Krieger-Liszka, A., Fufezan, C. & Trebst, A. Singlet oxygen production in photosystem II and related protection mechanism. *Photosynthesis Research* **98**, 551–564, <https://doi.org/10.1007/s1120-008-9349-3> (2008).
- Vass, I. Molecular mechanisms of photodamage in the Photosystem II complex. *Biochim Biophys Acta* **1817**, 209–217, <https://doi.org/10.1016/j.bbabi.2011.04.014> (2012).
- Pospíšil, P. Molecular mechanisms of production and scavenging of reactive oxygen species by photosystem II. *Biochim Biophys Acta* **1817**, 218–231, <https://doi.org/10.1016/j.bbabi.2011.05.017> (2012).
- Flors, C. *et al.* Imaging the production of singlet oxygen *in vivo* using a new fluorescent sensor, Singlet Oxygen Sensor Green. *J Exp Bot* **57**, 1725–1734, <https://doi.org/10.1093/jxb/erj181> (2006).
- Prasad, A., Ferretti, U., Sedlářová, M. & Pospíšil, P. Singlet oxygen production in *Chlamydomonas reinhardtii* under heat stress. *Scientific Reports* **6**, 20094, <https://doi.org/10.1038/srep20094> (2016).
- Prasad, A., Sedlářová, M., Kale, R. S. & Pospíšil, P. Lipoxygenase in singlet oxygen generation as a response to wounding: *in vivo* imaging in *Arabidopsis thaliana*. *Scientific Reports* **7**, <https://doi.org/10.1038/s41598-017-09758-1> (2017).
- Apel, K. & Hirt, H. Reactive oxygen species: metabolism, oxidative stress, and signal transduction. *Annual Review of Plant Biology* **55**, 373–399, <https://doi.org/10.1146/annurev.arplant.55.031903.141701> (2004).
- Laloi, C. & Havaux, M. Key players of singlet oxygen-induced cell death in plants. *Frontiers in Plant Science* **6**, <https://doi.org/10.3389/fpls.2015.00039> (2015).
- Gollan, P. J., Tikkanen, M. & Aro, E.-M. Photosynthetic light reactions: integral to chloroplast retrograde signalling. *Current Opinion in Plant Biology* **27**, 180–191, <https://doi.org/10.1016/j.pbi.2015.07.006> (2015).
- Aro, E. M. *et al.* Dynamics of photosystem II: a proteomic approach to thylakoid protein complexes. *Journal of Experimental Botany* **56**, 347–356, <https://doi.org/10.1093/jxb/eri041> (2005).
- Triantaphylides, C. *et al.* Singlet oxygen is the major reactive oxygen species involved in photooxidative damage to plants. *Plant Physiology* **148**, 960–968, <https://doi.org/10.1104/pp.108.125690> (2008).
- Pospíšil, P. & Yamamoto, Y. Damage to photosystem II by lipid peroxidation products. *Biochimica Et Biophysica Acta-General Subjects* **1861**, 457–466, <https://doi.org/10.1016/j.bbagen.2016.10.005> (2017).
- Mattila, H., Khorobrykh, S., Havurinne, V. & Tyystjärvi, E. Reactive oxygen species: Reactions and detection from photosynthetic tissues. *Journal of Photochemistry and Photobiology B-Biology* **152**, 176–214, <https://doi.org/10.1016/j.jphotobiol.2015.10.001> (2015).
- Koh, E. & Fluhr, R. Singlet oxygen detection in biological systems: Uses and limitations. *Plant Signaling & Behavior* **11**, 5, <https://doi.org/10.1080/15592324.2016.1192742> (2016).
- Hideg, E., Spetea, C. & Vass, I. Singlet Oxygen Production In Thylakoid Membranes During Photoinhibition As Detected by Epr Spectroscopy. *Photosynthesis Research* **39**, 191–199, <https://doi.org/10.1007/bf00029386> (1994).
- Krieger, A., Rutherford, A. W., Vass, I. & Hideg, E. Relationship between activity, D1 loss, and Mn binding in photoinhibition of photosystem II. *Biochemistry* **37**, 16262–16269, <https://doi.org/10.1021/bi981243v> (1998).
- Yadav, D. K. & Pospíšil, P. Evidence on the Formation of Singlet Oxygen in the Donor Side Photoinhibition of Photosystem II: EPR Spin-Trapping Study. *PLoS One* **7**, <https://doi.org/10.1371/journal.pone.0045883> (2012).
- Hideg, E. A comparative study of fluorescent singlet oxygen probes in plant leaves. *Central European Journal of Biology* **3**, 273–284, <https://doi.org/10.2478/s11535-008-0018-5> (2008).
- Hideg, E., Kalai, T., Kos, P. B., Asada, K. & Hideg, K. Singlet oxygen in plants- Its significance and possible detection with double (fluorescent and spin) indicator reagents. *Photochemistry and Photobiology* **82**, 1211–1218, <https://doi.org/10.1562/2006-02-06-ra-797> (2006).

25. Ragas, X., Jimenez-Banzo, A., Sanchez-Garcia, D., Batllori, X. & Nonell, S. Singlet oxygen photosensitisation by the fluorescent probe Singlet Oxygen Sensor Green (R). *Chemical Communications*, 2920–2922, <https://doi.org/10.1039/b822776d> (2009).
26. Gollmer, A. *et al.* Singlet Oxygen Sensor Green (R): Photochemical Behavior in Solution and in a Mammalian Cell. *Photochemistry and Photobiology* **87**, 671–679, <https://doi.org/10.1111/j.1751-1097.2011.00900.x> (2011).
27. Kim, S., Fujitsuka, M. & Majima, T. Photochemistry of Singlet Oxygen Sensor Green. *Journal of Physical Chemistry B* **117**, 13985–13992, <https://doi.org/10.1021/jp406638g> (2013).
28. Mor, A. *et al.* Singlet Oxygen Signatures Are Detected Independent of Light or Chloroplasts in Response to Multiple Stresses. *Plant Physiology* **165**, 249–261, <https://doi.org/10.1104/pp.114.236380> (2014).
29. Pedersen, S. K. *et al.* Aarhus Sensor Green: A Fluorescent Probe for Singlet Oxygen. *Journal of Organic Chemistry* **79**, 3079–3087, <https://doi.org/10.1021/jo500219y> (2014).
30. Frausto, F. & Thomas, S. W. Ratiometric Singlet Oxygen Detection in Water Using Acene-Doped Conjugated Polymer Nanoparticles. *ACS Applied Materials & Interfaces* **9**, 15768–15775, <https://doi.org/10.1021/acsami.7b02034> (2017).
31. Erbas-Cakmak, S. & Akkaya, E. U. Toward Singlet Oxygen Delivery at a Measured Rate: A Self-Reporting Photosensitizer. *Organic Letters* **16**, 2946–2949, <https://doi.org/10.1021/ol501084n> (2014).
32. Tang, C. Y. *et al.* A Classic Near-Infrared Probe Indocyanine Green for Detecting Singlet Oxygen. *Int J Mol Sci* **17**, 219, <https://doi.org/10.3390/ijms17020219> (2016).
33. Rippka, R., Deruelles, J., Waterbury, J. B., Herdman, M. & Stanier, R. Y. Generic Assignments, Strain Histories and Properties of Pure Cultures of Cyanobacteria. *Journal of General Microbiology* **111**, 1–61, <https://doi.org/10.1099/00221287-111-1-1> (1979).
34. Prasad, A. & Pospíšil, P. Linoleic Acid-Induced Ultra-Weak Photon Emission from *Chlamydomonas reinhardtii* as a Tool for Monitoring of Lipid Peroxidation in the Cell Membranes. *Plos One* **6**, e22345, <https://doi.org/10.1371/journal.pone.0022345> (2011).
35. Sedlářová, M. *et al.* Influence of nitric oxide and reactive oxygen species on development of lettuce downy mildew in *Lactuca* spp. *European Journal of Plant Pathology* **129**, 267–280, <https://doi.org/10.1007/s10658-010-9626-9> (2011).
36. Ogilby, P. R. Singlet oxygen: there is indeed something new under the sun. *Chemical Society Reviews* **39**, 3181–3209, <https://doi.org/10.1039/b926014p> (2010).
37. Hideg, E. & Ayaydin, F. In *Plant Image Analysis: Fundamentals and Applications* 265–277 (Crc Press-Taylor & Francis Group, 2015).
38. Sedlářová, M. & Luhová, L. Re-Evaluation of Imaging Methods of Reactive Oxygen and Nitrogen Species in Plants and Fungi: Influence of Cell Wall Composition. *Frontiers in Physiology* **8**, 7, <https://doi.org/10.3389/fphys.2017.00826> (2017).
39. Probes, M. Product information, <http://probes.invitrogen.com/media/pis/mp36002.pdf?id=;mp36002>. (2014).
40. Shen, Y. *et al.* Indirect imaging of singlet oxygen generation from a single cell. *Laser Physics Letters* **8**, 232–238, <https://doi.org/10.1002/lapl.201010113> (2011).
41. Sinha, R. K., Komenda, J., Knoppova, J., Sedlářová, M. & Pospíšil, P. Small CAB-like proteins prevent formation of singlet oxygen in the damaged photosystem II complex of the cyanobacterium *Synechocystis* sp PCC 6803. *Plant Cell and Environment* **35**, 806–818, <https://doi.org/10.1111/j.1365-3040.2011.02454.x> (2012).
42. Dall'Osto, L., Fiore, A., Cazzaniga, S., Giuliano, G. & Bassi, R. Different roles of alpha- and beta-branch xanthophylls in photosystem assembly and photoprotection. *Journal of Biological Chemistry* **282**, 35056–35068, <https://doi.org/10.1074/jbc.M704729200> (2007).
43. Alboresi, A. *et al.* Reactive oxygen species and transcript analysis upon excess light treatment in wild-type *Arabidopsis thaliana* vs a photosensitive mutant lacking zeaxanthin and lutein. *Bmc Plant Biology* **11**, 22, <https://doi.org/10.1186/1471-2229-11-62> (2011).
44. Ramel, F. *et al.* Chemical Quenching of Singlet Oxygen by Carotenoids in Plants. *Plant Physiology* **158**, 1267–1278, <https://doi.org/10.1104/pp.111.182394> (2012).
45. Ballottari, M., Mozzo, M., Girardon, J., Hienerwadel, R. & Bassi, R. Chlorophyll Triplet Quenching and Photoprotection in the Higher Plant Monomeric Antenna Protein Lhcb5. *Journal of Physical Chemistry B* **117**, 11337–11348, <https://doi.org/10.1021/jp402977y> (2013).
46. Shumbe, L. *et al.* Singlet Oxygen-Induced Cell Death in *Arabidopsis* under High-Light Stress Is Controlled by OX11 Kinase. *Plant Physiology* **170**, 1757–1771, <https://doi.org/10.1104/pp.15.01546> (2016).
47. Rehman, A. U., Cser, K., Sass, L. & Vass, I. Characterization of singlet oxygen production and its involvement in photodamage of Photosystem II in the cyanobacterium *Synechocystis* PCC 6803 by histidine-mediated chemical trapping. *Biochimica Et Biophysica Acta-Bioenergetics* **1827**, 689–698, <https://doi.org/10.1016/j.bbabi.2013.02.016> (2013).
48. Rehman, A. U. *et al.* Symbiodinium sp cells produce light-induced intra- and extracellular singlet oxygen, which mediates photodamage of the photosynthetic apparatus and has the potential to interact with the animal host in coral symbiosis. *New Phytologist* **212**, 472–484, <https://doi.org/10.1111/nph.14056> (2016).
49. Jurgens, U. J. & Weckesser, J. Polysaccharide Covalently Linked to the Peptidoglycan of the Cyanobacterium *Synechocystis* Sp Strain-Pcc6714. *Journal of Bacteriology* **168**, 568–573 (1986).
50. Foster, J. S., Havemann, S. A., Singh, A. K. & Sherman, L. A. Role of mrgA in peroxide and light stress in the cyanobacterium *Synechocystis* sp PCC 6803. *Fems Microbiology Letters* **293**, 298–304, <https://doi.org/10.1111/j.1574-6968.2009.01548.x> (2009).

## Acknowledgements

We thank Prof. Josef Komenda for providing *Synechocystis* cells and Dr. Marek Rác for discussions regarding SOSG infiltration in *Arabidopsis* leaves. This work was financially supported by the Ministry of Education, Youth and Sports of the Czech Republic Grant No. LO1204 (National Program of Sustainability I) and Palacký University, Olomouc, Czech Republic Grant No. IGA\_PrF\_2018\_001.

## Author Contributions

A.P., M.S., and P.P. contributed to the conception and design of the work. A.P. and M.S. performed the experiments. A.P., M.S., and P.P. drafted the manuscript and all authors approved the final version of the manuscript. PP overviewed the project.

## Additional Information

**Supplementary information** accompanies this paper at <https://doi.org/10.1038/s41598-018-31638-5>.

**Competing Interests:** The authors declare no competing interests.

**Publisher's note:** Springer Nature remains neutral with regard to jurisdictional claims in published maps and institutional affiliations.



**Open Access** This article is licensed under a Creative Commons Attribution 4.0 International License, which permits use, sharing, adaptation, distribution and reproduction in any medium or format, as long as you give appropriate credit to the original author(s) and the source, provide a link to the Creative Commons license, and indicate if changes were made. The images or other third party material in this article are included in the article's Creative Commons license, unless indicated otherwise in a credit line to the material. If material is not included in the article's Creative Commons license and your intended use is not permitted by statutory regulation or exceeds the permitted use, you will need to obtain permission directly from the copyright holder. To view a copy of this license, visit <http://creativecommons.org/licenses/by/4.0/>.

© The Author(s) 2018